1 **Mississippi river chemistry impacts on the interannual variability of aragonite**

2 **saturation state in the Northern Gulf of Mexico**

3

4 **Fabian A. Gomez[1,2], Rik Wanninkhof[2], Leticia Barbero[3,2], Sang-Ki Lee[2]**

5 [1]Northern Gulf Institute, Mississippi State University, Starkville, Mississippi, USA.

6 [2]NOAA Atlantic Oceanographic and Meteorological Laboratory, Miami, Florida, USA.

7 [3]Cooperative Institute for Marine and Atmospheric Studies, University of Miami, Miami,

8 Florida, USA.

9 Corresponding author: Fabian A. Gomez (fabian.gomez@noaa.gov)

10

11 **Key Points:**

12 • We simulated the Mississippi River impacts on interannual patterns of aragonite

13 saturation (Ω_{Ar}) in the northern Gulf of Mexico

14 • High-discharge conditions increase the frequency of suboptimal Ω_{Ar} levels for coastal

15 calcifying species in all seasons

16 • Reduced Ω_{Ar} under high-discharge is linked to low buffer capacity of riverine water in

17 winter and enhanced bottom remineralization in summer

18 **Abstract**

19 In the northern Gulf of Mexico shelf, the Mississippi-Atchafalaya River System (MARS)

20 impacts the carbonate system by delivering freshwater with a distinct seasonal pattern in both

21 total alkalinity (Alk) and dissolved inorganic carbon (DIC), and promoting biologically-driven

22 changes in DIC through nutrient inputs. However, how and to what degree these processes

23 modulate the interannual variability in calcium carbonate solubility have been poorly

24 documented. Here, we use an ocean-biogeochemical model to investigate the impact of MARS's

25 discharge and chemistry on interannual anomalies of aragonite saturation state (Ω_{Ar}). Based on

26 model results, we show that the enhanced mixing of riverine waters with a low buffer capacity

27 (low Alk-to-DIC ratio) during high-discharge winters promotes a significant Ω_{Ar} decline over the

28 inner-shelf. We also show that increased nutrient runoff and vertical stratification during high-

29 discharge summers promotes strong negative anomalies in bottom Ω_{Ar}, and less intense but

30 significant positive anomalies in surface Ω_{Ar}. Therefore, increased MARS discharge promotes an

31 increased frequency of suboptimal Ω_{Ar} levels for nearshore coastal calcifying species. Additional

32 sensitivity experiments further show that reductions in the Alk-to-DIC ratio and nitrate

33 concentration from the MARS significantly modify the simulated Ω_{Ar} spatial patterns, weakening

34 the positive surface Ω_{Ar} anomalies during high-discharge summers or even producing negative

35 surface Ω_{Ar} anomalies. Our findings suggest that riverine water carbonate chemistry is a main

36 driver of interannual variability in Ω_{Ar} over river dominated ocean margins.

37 **Plain Language Summary**

38 The Mississippi-Atchafalaya River System (MARS) influences coastal ocean acidity by

39 delivering freshwater with a distinctive seasonal signature in dissolved inorganic carbon (DIC)

40 and total alkalinity (Alk), and by promoting biological changes that impact the DIC distribution.

41 However, how and to what degree these two aspects modulate the spatiotemporal variability in

42 the solubility of calcium carbonate ($CaCO_3$), a key compound for marine calcifying organisms

43 such as shellfish and corals, remain poorly understood. Here, we use an ocean-biogeochemical

44 model to investigate the impacts of changes in river discharge and chemistry on the year-to-year

45 variability in $CaCO_3$ solubility over the northern Gulf of Mexico shelf. Model outputs show an

46 increased $CaCO_3$ solubility during high-discharge winters, mainly due to the mixing of riverine

47 waters with a low buffer capacity against acidification (i.e., low Alk-to-DIC ratio). The model

48   also shows that biological changes on DIC drive a more pronounced seasonal increase in bottom

49   $CaCO_3$ solubility during high-discharge summers. Our findings suggest that increased $CaCO_3$

50   solubility during high-discharge periods promotes suboptimal conditions for the growth and

51   development of calcifying organisms near the MARS delta. Additional analysis further shows

52   that interannual $CaCO_3$ solubility changes are impacted by the nutrient content and the Alk-to-

53   DIC ratio from riverine waters.

1 Introduction

55   Ocean Acidification (OA), caused by the ocean uptake of anthropogenic atmospheric

56   carbon dioxide (CO_2), is leading to a sustained decline in ocean pH, along with an increase in

57   partial pressure of CO_2 (pCO_2) and calcium carbonate solubility (Doney et al., 2009; Gruber et

58   al., 2019). These changes are exerting significant stress on marine species and ecosystems,

59   including negative impacts on growth and survival of calcifying organisms (e.g., Orr et al.,

60   2005). The rate of OA progression has significant spatial variability over continental margins,

61   where processes such as coastal upwelling, horizontal and vertical mixing, and river runoff can

62   strongly influence carbonate chemistry patterns (e.g., Duarte et al., 2013). In particular, rivers

63   play a relevant role, as they transport large amounts of freshwater, nutrients, carbon, and

64   alkalinity that affect inorganic carbon distribution and coastal acidity (e.g., Lacroix et al., 2020;

65   2021; Liu et al., 2021; Regnier et al., 2022). Understanding and constraining this river-induced

66   variability is needed to properly evaluate marine ecosystem vulnerability to OA progression.

67   The northern Gulf of Mexico (GoM) shelf is a river-dominated ocean margin, strongly

68   impacted by river runoff from the Mississippi-Atchafalaya River System (MARS). The nutrient

69   delivery from the MARS promotes enhanced phytoplankton production in the surface ocean

70   layer over the Louisiana-Texas shelf, which contributes to reduce dissolved inorganic carbon

71   (DIC), increase pH, and decrease pCO_2, the latter favoring an enhanced uptake of atmospheric

72   CO_2 (Lohrenz and Cai, 2006; Huang et al., 2015). The associated export of organic carbon to the

73   bottom layer and its remineralization decreases dissolved oxygen (DO) and releases CO_2,

74   promoting bottom hypoxia and acidification during summer (Rabalais et al., 2007; Cai et al.,

75   2011). Besides these biologically induced changes, the MARS has relatively high concentrations

76   of total alkalinity (Alk) and DIC compared to other rivers in the United States (Gomez et al.,

77   2023), which further influences ocean carbonate patterns. For example, high salinity-normalized

78   alkalinity in the northern GoM has been connected to the mixing of alkalinity-rich waters from

79   the MARS (Yang et al., 2015). However, an integrated description of the MARS's carbonate

80   chemistry impacts on the coastal ecosystem has remained largely overlooked. Particularly, it is

81   not well known how temporal changes in river Alk and river DIC impact the buffer capacity

82   nearshore. This could be a relevant aspect considering that Alk and DIC from the MARS have a

83   strong seasonal variability. Indeed, the annual amplitude for these two variables is about 600 and

84   800 µmol kg^{-1} for the Mississippi and Atchafalaya Rivers, respectively, which is substantially

85   larger than the seasonal variability in open ocean waters (Figure 1a–b).

86   Changes in pH, pCO$_2$, and aragonite saturation state (Ω_{Ar}), three regularly used OA

87   metrics, are driven by changes in temperature, salinity, Alk, and DIC. Ω_{Ar} represents the

88   solubility of aragonite, a specific mineral phase of CaCO$_3$, which can be defined by:

89        $$\Omega_{Ar} = [CO_3^{-2}] \cdot [Ca^{+2}] \cdot K_{Ar}^{-1} \tag{1}$$

90   where $[CO_3^{-2}]$ is the carbonate ion concentration, a propriety strongly correlated to the Alk-to-

91   DIC ratio (Alk:DIC ratio), $[Ca^{+2}]$ is the calcium ion concentration, which varies with salinity,

92   and K_{Ar} is the apparent solubility product of aragonite, a function of temperature, salinity, and

93   pressure (Wang et al., 2013; Wanninkhof et al., 2015). Aragonite is prone to dissolve at Ω_{Ar}

94   values lower than one, but calcifying organisms may start experiencing stress under Ω_{Ar} values

95   lower than 2.0 (e.g., Siedlecki et al., 2021; Kekuewa et al., 2022). Quantifying the occurrence of

96   those suboptimal levels is therefore relevant for the management of shellfish and other important

97   marine resources. Previous studies have reported a marked decline in bottom Ω_{Ar} near the MARS

98   delta during summer, concurrent with bottom hypoxia (Cai et al., 2011; Laurent et al., 2017).

99   However, year-to-year changes in coastal Ω_{Ar} patterns have been poorly described, and

100   relationships linking MARS discharge to Ω_{Ar} anomalies have not been yet established. As such,

101   coastal ecosystem vulnerability to suboptimal Ω_{Ar} conditions in the region remains uncertain.

102   Further understanding of the carbonate system responses to changes in river runoff is

103   important to assess regional vulnerabilities to OA. To this goal, high-resolution ocean

104   biogeochemical (BGC) models that simulate carbon dynamics can provide valuable insights. In

105   the present study we used outputs from an ocean-BGC model configured by Gomez et al. (2020)

106   to examine the carbonate system response to changes in MARS discharge and chemistry. To this

107   effect, we characterize the simulated interannual anomaly patterns for salinity, Alk, DIC, and Ω_{Ar}

108   during high and low MARS discharge periods, identifying the main underlying factors

109   modulating those anomalies. We then performed a sensitivity analysis to investigate to what

110   degree changes in MARS chemistry could modify the link between MARS discharge and

111   interannual Ω_{Ar} variability. Finally, we derived frequency histograms for Ω_{Ar} under high and low

112   MARS discharge conditions, quantifying the fraction of suboptimal Ω_{Ar} levels for calcifying
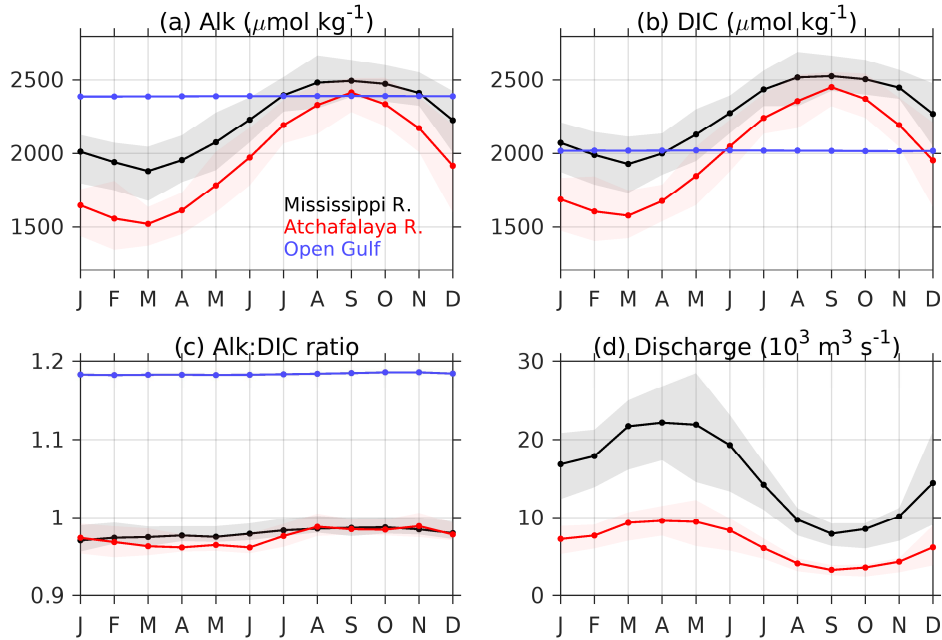
113   organisms.

Figure 1. MARS monthly climatologies during 1980-2019: (a) alkalinity (Alk), (b) dissolved inorganic carbon (DIC), (c) alkalinity-to-DIC ratio (Alk:DIC ratio), and (d) discharge for the Mississippi (black) and Atchafalaya (red) rivers. Interquartile intervals are also depicted as gray and light red shadows, respectively. Simulated surface alkalinity, DIC, and Alk:DIC ratio over open Gulf waters are shown in blue for comparison with river patterns.

2 Materials and Methods

115   The ocean-biogeochemical model, referred to as GoMBio, simulates 16 state variables,

116   including Alk and DIC. It was built up in the Regional Ocean Model System (ROMS;

117   Shchepetkin and McWilliams, 2005), with a horizontal resolution of 8 km and 37 sigma-

118   coordinate vertical levels. Initial and open boundary conditions were derived from a 25 km

119   horizontal resolution model for the North Atlantic (Liu et al., 2015). Surface fluxes of

120   momentum, heat, and freshwater were derived from the ERA5 reanalysis product (Hersbach et

121   al., 2020) using bulk flux parameterizations. Daily river discharge for U.S. rivers was obtained

122   from the U.S. Army Corps of Engineers and U.S. Geological Survey (USGS) records, available

123   at the Gulf of Mexico Coastal Ocean Observing System (https://geo.gcoos.org/river_discharge/).

124   River chemistry for U.S. rivers was obtained from RC4USCoast (Gomez et al., 2023), a river

125   chemistry dataset based on the USGS Water Quality Database. Discharge and chemistry data for

126   Mexican rivers were derived from the scientific literature (e.g., Munoz-Salinas and Castillo,

127   2015; Martinez-Lopez and Zavala-Hidalgo, 2009). Further model details can be found in Gomez

128   *et al.* (2020).

129   To investigate the impact of interannual changes in MARS runoff on the carbonate

130   system variability, we conducted a composite analysis of the mean detrended anomalies of

131   salinity, DIC, Alk, and Ω_{Ar} during high and low discharge conditions (hereinafter anomaly

132   implies a monthly model output with the monthly climatology average subtracted). To account

133   for seasonal variation in the carbonate system response to runoff changes, independent

134   composites were generated for winter (December-February), spring (March-May), summer

135   (June-August), and fall (September-November). The percentiles 75% and 25% of seasonal

136   averaged MARS discharge series were used as thresholds to define high and low discharge

137   periods, respectively. The seasonally averaged discharge series were derived from daily

138   discharge observations, and led the anomaly composite for one week to account for a lagged

139   phytoplankton response to runoff changes. For example, the winter averaged discharge series

140   integrated observations from the last week of November to the third week of February. The

141   selected composite's years for each season (10 years) are reported in Table S1 from the

142   Supplementary Material. The statistical significance of the composites was assessed with Monte

143   Carlo experiments (von Storch and Zwiers, 1999). For each variable, 1,000 independent

144   realizations of the composite were generated by randomly selecting 10 years from 1980–2019. A

145   composite anomaly was significant at the 90% level when it fell outside the interval defined by

146   the percentiles of 5% and 95% from the randomly generated composite distribution.

147   To investigate the role of Alk, DIC, salinity (S), and temperature (T) as main underlying

148   drivers of Ω_{Ar} variability, we performed a first order Taylor series decomposition:

149    $$\Delta\Omega_{Ar} \approx \frac{\partial \Omega_{Ar}}{\partial Alk} \cdot \Delta Alk + \frac{\partial \Omega_{Ar}}{\partial DIC} \cdot \Delta DIC + \frac{\partial \Omega_{Ar}}{\partial S} \cdot \Delta S + \frac{\partial \Omega_{Ar}}{\partial T} \cdot \Delta T \qquad (2)$$

150   Where $\Delta\Omega_{Ar}$ represents the temporal change for Ω_{Ar}, and the four right side terms in equation (2)

151   represent the Alk, DIC, salinity and temperature contribution to the Ω_{Ar} change, respectively.

152   The partial derivatives of the contribution terms were calculated by adding a small perturbation

153   to each driver while keeping the other three terms as constant, using the CO2SYS program for

154   CO_2 System Calculations (van Heuven et al., 2011).

155   In addition to the model hindcast, we conducted five experiments to evaluate the

156   carbonate system sensitivity to changes in MARS chemistry (Table S2 in the Supplement). In the

157   Constant Carbonate (CCBN) experiment, we used long-term (1980-2019) averages for the

158   Mississippi and Atchafalaya Alk (1,956 and 2,215 µmol kg^{-1}, respectively) and DIC (2,002 and

159   2,258 µmol kg^{-1}, respectively) instead of time evolving patterns. In the Alk090 and Alk110

160   experiments, the MARS's Alk was reduced and increased by 10%, respectively (i.e., an average

161   Alk increase/decrease of about 196 mmol kg^{-1} for the Atchafalaya River, and 222 mmol kg^{-1} for

162   the Mississippi River). Finally, in the N80 and N50, the MARS's nitrate concentration (about 83

163   µmol kg^{-1} during 1980-2019) was decreased by 20% and 50%, respectively. N50 represents an

164   important decrease in nitrate concentration (about 40 mmol kg^{-1}), which could be connected to

165   the nitrogen load reduction target of 45% set by the Hypoxia Task Force to mitigate bottom

166   hypoxia (www.epa.gov/ms-htf; last access: September 2023).

167   **3 Results**

168   3.1 Composite analysis

169   Figure 2 shows the surface and bottom composites for salinity, Alk, and DIC under high

170   MARS discharge conditions. The salinity patterns revealed a significant coastal freshening,

171   which was mostly constrained to the inner-shelf (bottom depth < 25 m), with surface and bottom

172   salinity (SSS and *b*Sal) anomalies reaching magnitudes greater than 1.5 and 0.5, respectively,

173   near the MARS delta (Figures 2a and 2d). The coastal freshening was concurrent with a

174   significant decrease in surface and bottom Alk (*s*Alk and *b*Alk) during winter-spring, with the

175   largest anomaly magnitude exceeding 25 and 15 µmol kg^{-1}, respectively (Figures 2b and 2e). In

176   contrast, the Alk anomalies were mostly not significant during summer-fall (Figures 2b and 2e).

177   To some degree, the surface DIC (*s*DIC) pattern resembled that for *s*Alk (Figure 2c), but with

178   weaker anomalies in winter-spring, and significant positive anomalies near the Mississippi

179   mouth in summer-fall (Figure 2c). On the other hand, the bottom DIC (*b*DIC) patterns largely
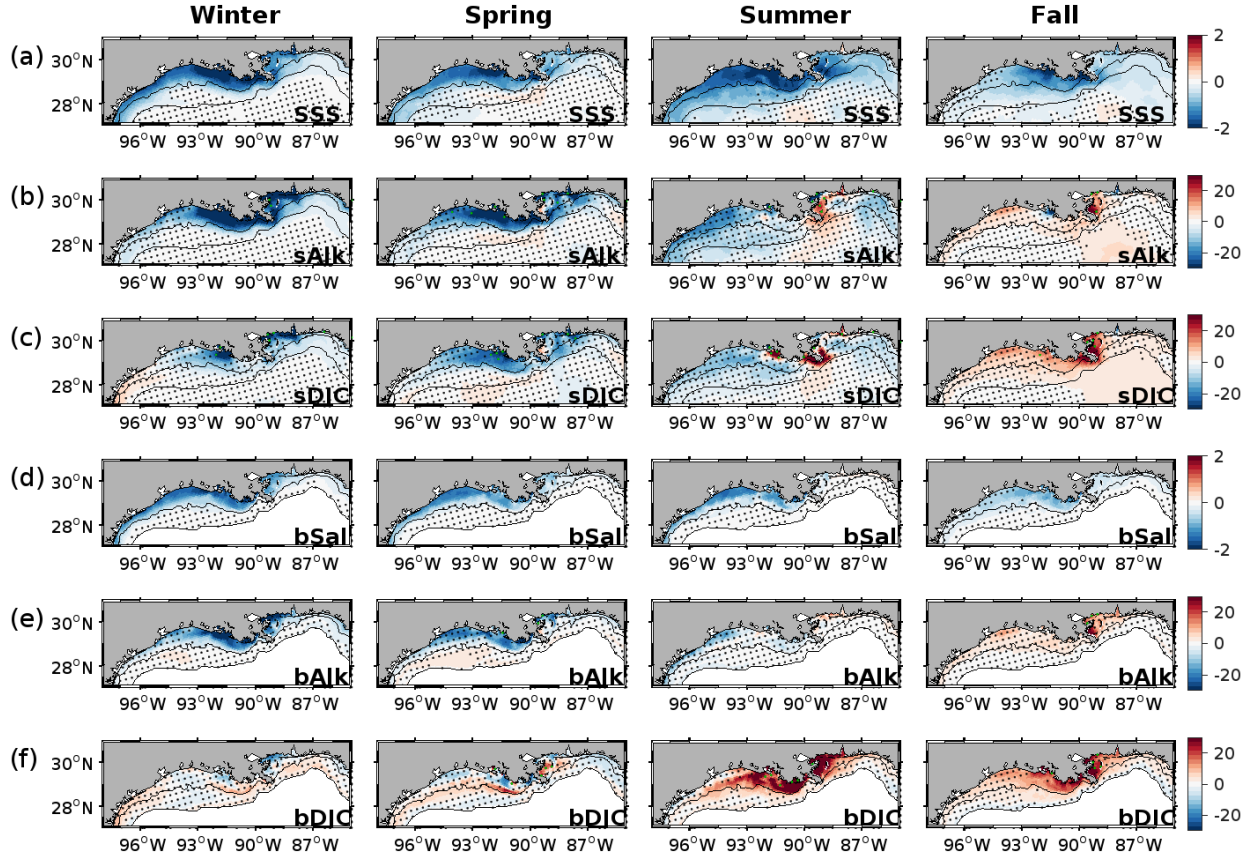
Figure 2. High discharge composites of the hindcast anomalies of (a) sea surface salinity (SSS), (b) surface alkalinity (*s*Alk), (c) surface DIC (*s*DIC), (d) bottom salinity (*b*Sal), (e) bottom alkalinity *(b*Alk), and (f) bottom DIC (*b*DIC) during winter, spring, summer, and fall. Anomaly series were detrended before estimating the composites. Black contours depict the 25 m and 200 m isobaths. Alkalinity and DIC anomalies are in µmol kg^{-1}. Dotted area represents non-significant values.

180   differed from the *b*Alk pattern, showing significant positive anomalies during summer-fall,

181   which exceeded 30 µmol kg^{-1} near the delta (Figure 2f).

182   The significant *s*Alk decline during high discharge winters and springs can be linked to a

183   strong MARS dilution effect on Alk, as the MARS' Alk was substantially lower than the open

184   ocean Alk (<2,000 µmol kg^{-1}). This was connected with a flow-dependent seasonal variability in

185   river alkalinity, which displayed a minimum in late-winter and early-spring (Figures 1a and 1d),

186   and a negative relationship between discharge and river alkalinity at the interannual timescale,

187   which was especially strong during winter (Figure S1 in the Supplement). Similarly, the sDIC

188   anomalies during high discharge conditions were influenced by seasonal and interannual changes

189   in MARS's DIC (Figure 1b; Figures S1 in the Supplement), which promoted a prevailing

190   dilution effect during winter-spring (but weaker compared to that for sAlk), and an enrichment

191   effect during summer-fall. On top of this variability, an enhanced biological uptake of DIC,

192   reflected in positive surface net community production (NCP, which is the difference between

193   primary production and respiration) and dissolved oxygen (produced by photosynthesis)

194   anomalies (Figures S2a and S2b in the Supplement), contributed to reinforce the river dilution

195   signal in winter-spring, and counteract the river enrichment in summer-fall (more details in

196   Section 3.2). sDIC was further impacted by changes in air-sea CO_2 fluxes, with an increased

197   outgassing near Mississippi and Atchafalaya mouths, and carbon uptake over part of the inner-

198   shelf (Figures S2c in the Supplement). But the changes in the magnitude of the air-sea CO_2

199   fluxes were relatively small compared to the biologically-induced changes. High discharge

200   conditions also promoted respiration leading to negative bottom NCP and dissolved oxygen

201   anomalies, reflecting increased bottom remineralization in the four seasons (Figure S2d–e in the

202   Supplement). During summer, the strong bottom oxygen decrease mirrors the strong bDIC

203   increases (Figure 2f), indicative of increased bottom acidification due to strong vertical

204   stratification.

205   The surface Ω_{Ar} ($s\Omega_{Ar}$) response to the MARS-induced changes in SSS, sAlk, and sDIC

206   displayed an important seasonal modulation (Figure 3a). Strong negative anomalies (>0.2 units)

207   prevailed over the inner-shelf during winter, while positive anomalies (>0.1 units) dominated in

208   part of the inner and outer shelf during summer. Strong negative anomalies also were found near

209   the Mississippi and Atchafalaya River mouths during spring-fall. Since $s\Omega_{Ar}$ near the delta is the

210   lowest in winter and highest in summer (Figure S3a in the Supplement), the derived anomaly

211   patterns imply a strengthening of both the seasonal minimum in winter and the seasonal

212   maximum in summer. The Taylor series decomposition (Eqn. 2) showed that the $s\Omega_{Ar}$

213   composite's anomalies were mainly determined by a balance between Alk- and DIC-induced

214   changes (Figure 3b–d). During winter, the strong Alk decrease dominated the Alk-DIC balance,

215   leading to a significant $s\Omega_{Ar}$ drop over the inner-shelf. During summer, the DIC-induced changes

216   prevailed over the central part of the northern GoM shelf, leading to negative anomalies near the

217   Mississippi and Atchafalaya mouths, and positive anomalies further away from the discharge
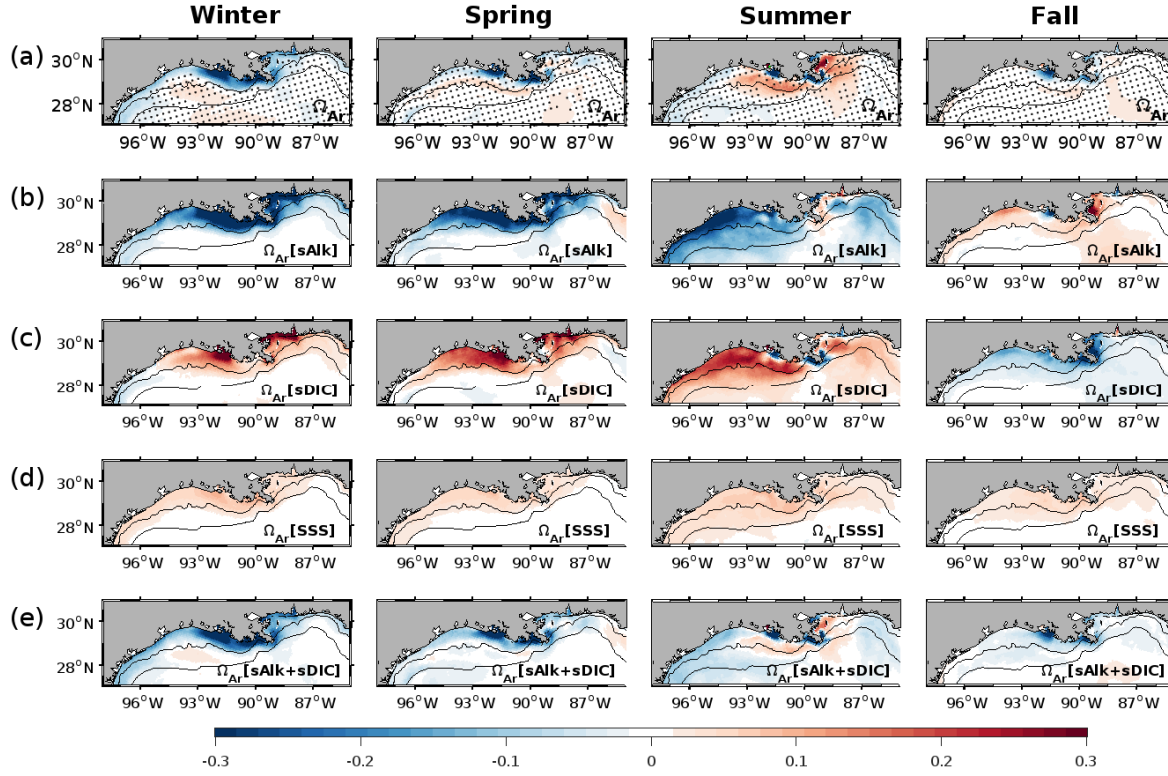
Figure 3. (a) High discharge composites of surface aragonite saturation during winters, springs, summers, and falls, as derived from the model hindcast; (b–e) Taylor decomposition terms of the composite's patterns, representing changes induced by (b) surface alkalinity (sAlk), (c) surface DIC, (d) sea surface salinity (SSS), and (e) the added effect of sAlk and sDIC. The temperature term was omitted since it has a residual impact in the composite. Anomaly series were detrended before estimating the composites. Dotted area in (a) represents non-significant anomalies. Black contours depict the 25 m and 200 m isobaths.

218 points. Surface freshening had a relatively weak positive impact on $s\Omega_{Ar}$, contributing to

219 attenuate the $s\Omega_{Ar}$ decline in winter, and accentuate the $s\Omega_{Ar}$ increase in summer. Temperature

220 driven changes were small and did not contribute significantly to the total anomaly (not shown).

221 In the bottom layer, the composite showed significant Ω_{Ar} decline over the inner-shelf in the four

222 seasons (Figure 4a), with the strongest anomalies in summer (>0.3 units). As bottom Ω_{Ar} ($b\Omega_{Ar}$)

223 near the delta is the lowest in summer (Figure S3b in the Supplement), the pattern implies a more

224 pronounced seasonal minimum during high-discharge summers. The Taylor decomposition for

225 the bottom Ω_{Ar} ($b\Omega_{Ar}$) anomalies indicated that changes in Alk in winter-spring, and DIC in

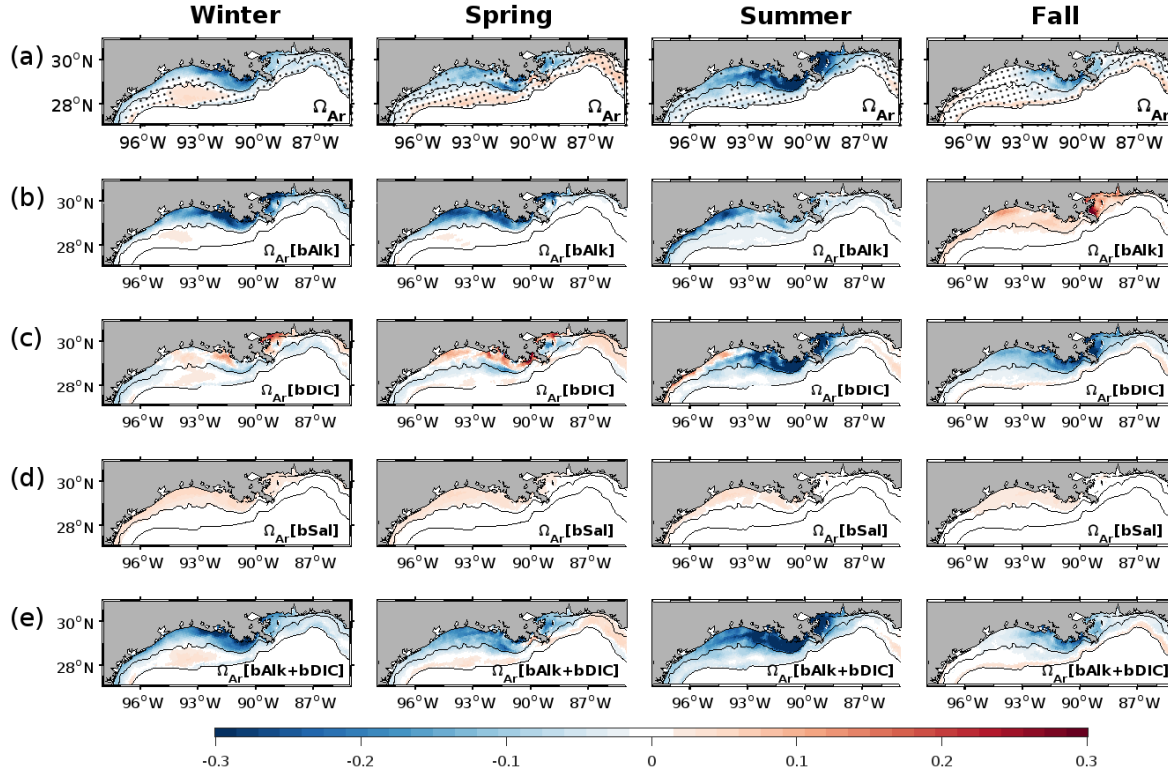226 summer-fall, led to those anomaly patterns (Figure 4b–d).

Figure 4. As Figure 3 but for bottom aragonite saturation state.

227   The carbonate system patterns during low discharge conditions were mostly opposite to

228   those in the high discharge scenarios (Figures S4–S7 in the Supplement). Significant positive

229   anomalies were obtained for sAlk, sDIC, and bAlk during winter-summer, and significant

230   negative anomalies for bDIC during summer. Besides, $s\Omega_{Ar}$ showed prevailing positive

231   anomalies in the inner-shelf during winter-spring, and a significant $s\Omega_{Ar}$ decline in part of the

232   inner and outer shelf during summer. Finally, the $b\Omega_{Ar}$ anomalies showed significant positive

233   values in the four seasons, with a maximum in summer.

234   3.2 Sensitivity analysis

235   The high discharge composites for Alk and DIC in the Constant Carbonate experiment

236   (CCBN; Table S2 in the Supplement) showed important differences with respect to the

237   hindcast's composites (Figure S8 in the Supplement). During winter-spring, we obtained a

238   weakening of the negative sAlk and bAlk anomalies, along with the emergence of positive sDIC

239   anomalies near the rivers' mouths, and positive bDIC anomalies over the inner-shelf. Also,

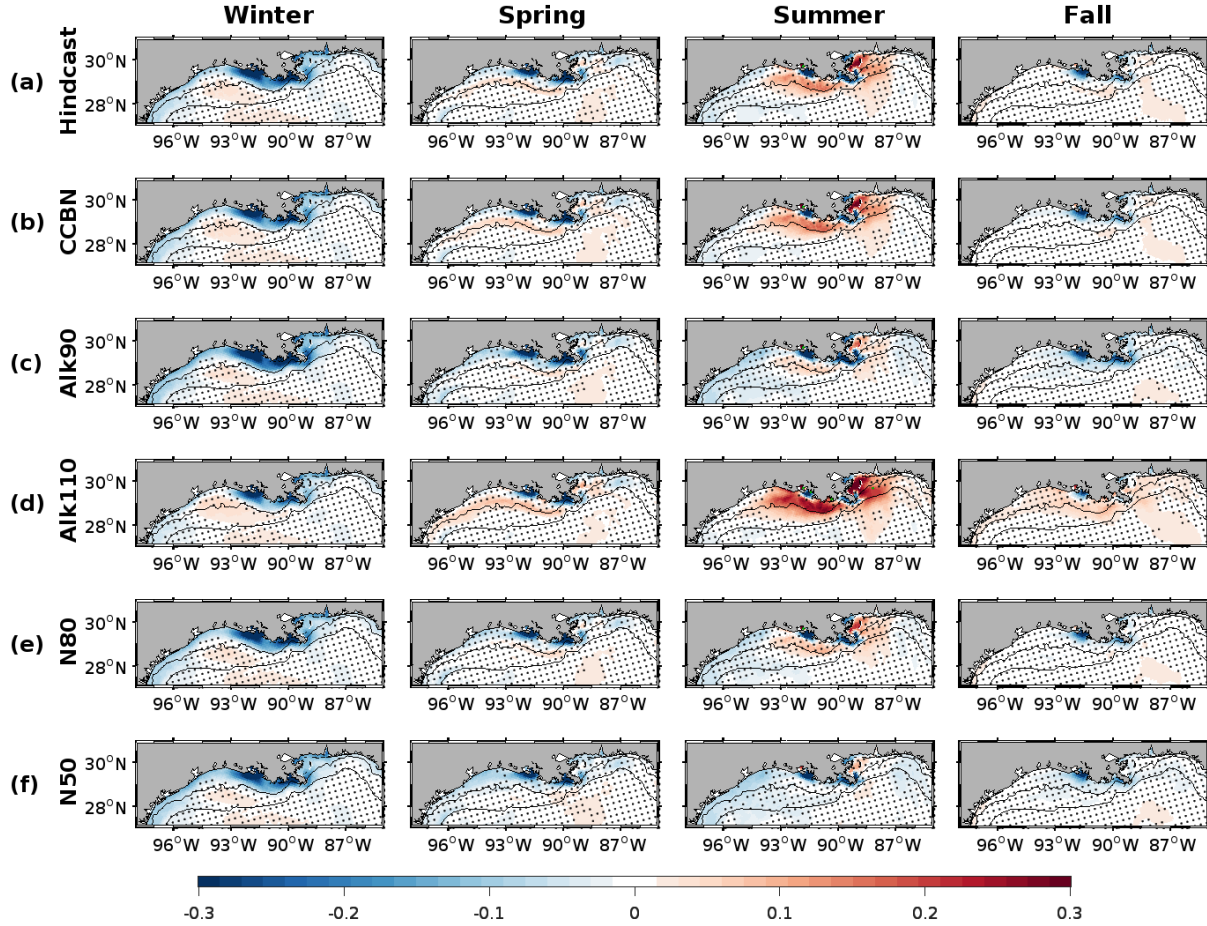240   during summer-fall, the positive sDIC anomalies weakened. Despite all those changes, the Ω_{Ar}

11

Figure 5. High discharge composites of the mean surface Ω_{Ar} anomaly derived from the following experiments: (a) Hindcast, (b) Constant carbonate (CCBN), (c) Alkalinity 90% (Alk90), (d) Alkalinity 110% (Alk110), (e) Nitrate 80% (N80), and (f) Nitrate 50% (N50). Anomaly series were detrended before estimating the composites. Black contours depict the 25 m and 200 m isobaths. Dotted area represents non-significant values.

241 anomalies for the CCBN experiment closely resembled those in the hindcast experiment (Figure

242 5a–b and Figures S9a and S9b in the Supplement). An examination of the Alk:DIC ratio from

243 MARS waters provides insight to explain the Ω_{Ar} pattern similarities. The Mississippi and

244 Atchafalaya Rivers are characterized by a strong seasonal variation in Alk and DIC, but the ratio

245 between these two variables has a weak annual variation, with an average and standard deviation

246 of about 0.98 and 0.02, respectively (Figure 1c). In the CCBN experiment, the interannual and

247 seasonal changes in MARS's Alk and DIC were removed, but the MARS's Alk:DIC ratio did not

248 depart significantly from the average hindcast value. The CCBN experiment then modified the

249   relationship between discharge and both coastal Alk and DIC, but it did not change the

250   relationship between discharge and the coastal Alk:DIC ratio. Thus, the balance between coastal

251   Alk and DIC was very similar (Figures S10e and S11e in the Supplement). Changes in the

252   MARS's Alk:DIC ratio did produce changes in the Ω_{Ar} anomalies. In the Alk90 experiment,

253   where the ratio was decreased by 10%, the significant positive $s\Omega_{Ar}$ anomalies vanished (Figure

254   5c). On the other hand, the Alk110 experiment, whose ratio was increased by 10%, displayed a

255   significant strengthening of the positive $s\Omega_{Ar}$ anomalies, especially evident in summer (Figure

256   5d). Changes in MARS nitrate concentration also impacted the Ω_{Ar} variability. A nitrate

257   reduction of 20% and 50%, as in the N80 and N50 experiments, largely weakened the $s\Omega_{Ar}$

258   positive anomalies in summer, as this implied a significant decrease in biological uptake (Figure

259   5e–f). Indeed, in the N50 experiment, an inverse relationship was obtained between MARS

260   discharge and $s\Omega_{Ar}$ in the four seasons.

261   To further illustrate the system responses to river runoff variability in the hindcast,

262   CCBN, and N50 experiments, we conducted a correlation analysis between MARS discharge and

263   simulated carbonate system variables around the MARS delta at surface, spatially-averaged from

264   93º to 90ºW and northward of 28.5ºN. We exclude from the spatial averaging locations with

265   salinity below 20, where the phytoplankton response to riverine nutrient was strongly light-

266   limited. This usually corresponded to a few data points near the Mississippi and Atchafalaya

267   mouths. Consistent with the composite analysis results, the correlation patterns for sAlk and

268   sDIC showed important differences between the hindcast and CCBN experiments (Figure 6a–b),

269   while the correlation between discharge and the surface Alk:DIC ratio was very similar (Figure

270   6c). It is worth noting that under conservative mixing, we would expect a negative correlation

271   between discharge and the Alk:DIC ratio near the delta year-round, since the average MARS

272   ratio was always smaller than the surface ocean ratio (~0.98 vs. 1.18). Consequently, the positive

273   correlation coefficients obtained during summer mainly reflect biological uptake of DIC

274   counteracting the low ratio signature from the MARS waters. Biology also explains the strong

275   seasonality in the discharge-sDIC correlation of the CCBN experiment, something not evident in

276   the hindcast sDIC, as the latter was also modulated by the river DIC seasonality. In the N50

277   experiment, the correlation patterns for sAlk and sDIC were similar to the hindcast patterns, but

278   the decreased biological uptake, linked to decreased riverine nutrient, led to a weaker

279 phytoplankton impact on the Alk:DIC ratio during summer (Figure 6c). Since Ω_{Ar} is modulated

280 by the Alk:DIC ratio, the discharge-Ω_{Ar} correlation pattern showed significant negative

281 coefficients in winter for the three experiments, and significant positive coefficients in summer

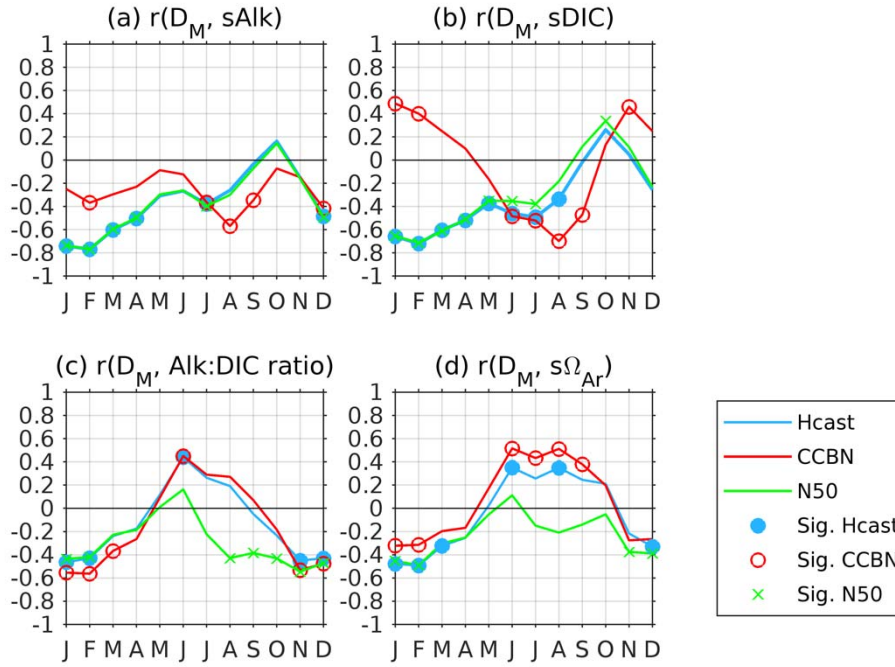282 for the hindcast and CCBN experiments (Figure 6d).

Figure 6. Monthly correlation coefficients between MARS discharge (D_M) and simulated spatially averaged series of surface alkalinity (sAlk), surface dissolved inorganic carbon (sDIC), surface alkalinity to DIC ratio (sADIC ratio), and surface aragonite saturation ($s\Omega_{Ar}$) over 93°–90°W and north of 28.0 °N, as derived from the hindcast (Hcast), Constant Carbonate (CCBN), and Nitrate 50% (N50) experiments. Carbon system variables were derived for locations with surface salinities greater than 20. All series were detrended before correlation.

283   3.3 Ω_{Ar} frequency distribution

284   The MARS-induced Ω_{Ar} anomalies described above implied changes in the probability

285 distribution function of Ω_{Ar} nearshore, which has the potential for a significant impact in

286 calcifying organisms. To evaluate this, we derived frequency histograms for $s\Omega_{Ar}$ and $b\Omega_{Ar}$, from

287 the hindcast and quantified the fraction of suboptimal values ($\Omega_{Ar} < 2$), over the inner shelf

288 region near the delta under high and low MARS discharge. To limit the impact of OA and other
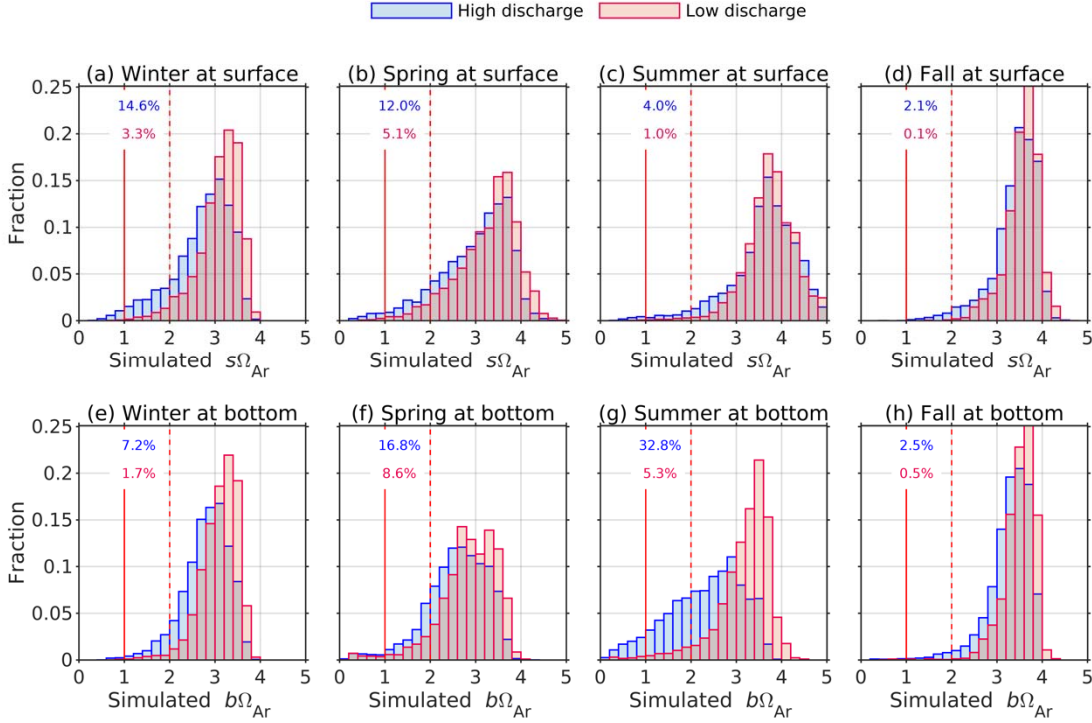
Figure 7. Frequency histograms for the simulated surface (a-d) and bottom (e-h) aragonite saturation state over the northern Gulf inner shelf (<25 m bottom depth; 93º–89ºW) during the high and low discharge conditions from 2000-2019: (a, e) winter, (b, f) spring, (c, g) summer, and (d-h) fall. Blue and red numbers at each panel indicate the percentage of suboptimal values ($\Omega_{Ar} < 2$) during high and low discharge, respectively.

289   low-frequency related changes in our calculations, independent estimates of histograms and

290   suboptimal fractions were derived for 1980-1999 and 2000-2019. We present below the patterns

291   for the latter period, but similar results were obtained for the former period (Table S3 and

292   Figures S12in the Supplement). The derived Ω_{Ar} histograms for 2000-2019 showed significant

293   differences between discharge scenarios, seasons, and vertical layers (Figure 7). Enhanced

294   MARS discharge increased the suboptimal fraction in all seasons. This is reflected in the ratio

295   between the suboptimal Ω_{Ar} fraction under high and low discharge conditions. At surface, that

296   ratio was 4.4, 2.4, 4.0, and 21.0 during winter, spring, summer, and fall, respectively. At bottom,

297   the same ratio was 4.2, 2.0, 6.2, and 5.0, respectively. The greatest portion of suboptimal $s\Omega_{Ar}$

298   values was 14.6% in winter, and the greatest portion of suboptimal $b\Omega_{Ar}$ was 32.8% in summer.

299   Moreover, during high discharge spring and summers, 2.6% and 7.4% of the $b\Omega_{Ar}$ values were

300 below one, which represents corrosive conditions for aragonite. Suboptimal Ω_{Ar} conditions were

301 infrequent in fall, corresponding to less than 3% of the outputs under high discharge.

302 We also calculated the suboptimal Ω_{Ar} fractions for our five sensitivity experiments

303 (Table S4). As expected from the previous results, the more meaningful differences from the

304 hindcast were associated with the Alk90, Alk110, N80, and N50 experiments. Alk90 promoted

305 about 50% increase in the suboptimal surface fraction during high-discharge winters and springs,

306 and about 20% increase in the suboptimal bottom fraction during high-discharge summers,

307 whereas Alk110 produced the opposite effects. In the case of the N80 and N50 experiments, the

308 main differences from the hindcast were obtained at bottom during high-discharge summers,

309 where the suboptimal fraction decreased by about 20% and 50%, respectively.

310 **4 Summary and Discussion**

311 A composite analysis of simulated carbonate system variables was conducted to describe

312 emerging anomaly patterns under high and low MARS discharge years. Our motivation was to

313 examine the impacts of river carbonate chemistry and nutrient runoff on the interannual Ω_{Ar}

314 variability. The model results showed an important seasonal variation in the relevance of these

315 two driving mechanisms. High discharge winters promoted negative $s\Omega_{Ar}$ and $b\Omega_{Ar}$ anomalies

316 near the MARS delta, mainly driven by the mixing of MARS waters with a low Alk:DIC ratio.

317 High discharge summers promoted strong negative $b\Omega_{Ar}$ anomalies and less intense but

318 significant positive $s\Omega_{Ar}$ anomalies, which were mainly associated with biological-changes

319 fostered by nutrient runoff and salinity-driven stratification. Previous studies in the northern

320 GoM showed that biological processes play an important role in the generation of bottom

321 acidification (e.g., Cai et al., 2011), and that the interaction between MARS carbonate chemistry

322 and biology influenced the spatial variability in surface Ω_{Ar} (e.g., Guo et al., 2012; Huang et al.,

323 2021). Our results are consistent with those studies, providing an extended framework that

324 includes discharge, the Alk:DIC ratio, and nutrients from the MARS as main parameters to

325 understand interannual patterns in the coastal carbonate system.

326 Our analysis of the USGS-derived river chemistry revealed an important temporal

327 variability in Alk and DIC from the MARS, which is inversely related to river discharge. This

328 flow-dependent pattern is a common feature in many riverine systems, associated with the

329   dilution of major river's solutes during high-discharge periods (Joesoef et al., 2017; Li et al.,

330   2022; Gomez et al., 2023). The seasonal changes in MARS's carbonate chemistry decreased both

331   Alk and DIC during winter-spring, and increased it during summer-fall. The flow-dependent

332   interannual anomalies in river Alk and river DIC reinforced the coastal dilution effect during

333   high-discharge winters and springs, producing significant negative anomalies in sAlk, bAlk, and

334   sDIC over the inner-shelf. However, since Alk and DIC from the MARS were highly correlated

335   (r = 0.99), the MARS's Alk:DIC ratio displayed a rather weak seasonal and interannual

336   variability, which was also unrelated to the river flow changes. The average MARS's Alk:DIC

337   ratio was about 17% lower than the surface open GoM values, which implies that the freshwater

338   contributed to decreasing the surface Ω_{Ar} values near the delta year-round, despite the relatively

339   high alkalinity values in the Mississippi River, greater than the ocean alkalinity values during

340   summer-fall. Sensitivity analysis revealed that the Ω_{Ar} anomalies are more responsive to changes

341   in the river Alk:DIC ratio than the seasonal changes in the magnitude of the river Alk and river

342   DIC concentrations. This is because the effect of Alk and DIC on Ω_{Ar} counteracted each other;

343   thus, the total Ω_{Ar} anomaly is largely determined by a small residual difference between the two

344   drivers. The low river Alk:DIC ratio is to some degree offset by enhanced biological uptake at

345   surface fostered by MARS's nutrient runoff. High-discharge conditions increase surface NCP

346   during the four seasons, but significant positive $s\Omega_{Ar}$ anomalies were only obtained in summer,

347   concurrent with the largest negative anomalies in $b\Omega_{Ar}$. This last pattern is linked to the strong

348   salinity-driven vertical stratification, which promotes a decoupling between phytoplankton

349   production in the upper layer and respiration below (Cai et al., 2011; Laurent et al., 2017). The

350   interannual Ω_{Ar} patterns are sensitive to changes in nitrate content, with decreased nitrate values

351   lessening or even reversing the positive $s\Omega_{Ar}$ anomalies during high-discharge summers.

352   The northern GoM shelf is a region characterized by a large spatiotemporal variability in

353   carbonate system variables, which added to the still limited length of observational records make

354   it difficult to discern interannual variation from long-term trend in pH, pCO_2, or Ω_{Ar} (e.g.,

355   Kealoha et al., 2020). Thus, the interannual variability and its modulation by the MARS runoff

356   have remained poorly documented, implying an important gap that limits our ability to quantify

357   the northern GoM ecosystem vulnerability to OA progression and other stressors. Our model

358   results suggest a greater prevalence of suboptimal Ω_{Ar} values near the MARS delta under high-

359   discharge periods. As bottom acidification is a seasonally recurring phenomena, the greatest

360   suboptimal Ω_{Ar} fraction near the bottom was obtained under high-discharge summers,

361   representing about one-third of the inner-shelf values near the MARS delta. Suboptimal

362   conditions were also simulated in the surface layer, especially under high-discharge winters,

363   representing about 15% of the inner-shelf values during 2000-2019. In comparison, the

364   corresponding suboptimal values under low-discharge summers and winters were 5% and 3%,

365   respectively. This indicates an enhanced vulnerability of calcifying organisms under flooding

366   conditions, which are expected to increase their frequency due to climate change (Tao et al.,

367   2014; Hicks et al., 2022). Our sensitivity experiments revealed significant changes in the

368   suboptimal Ω_{Ar} fractions associated with minor variations in river alkalinity (representing ±10%

369   variations in the river Alk:DIC ratio) and reduction in river nitrate. In addition, a 50% reduction

370   in river nitrate led to a 50% decrease in the suboptimal bottom Ω_{Ar} fraction on the inner-shelf

371   near the MARS delta. This result highlights the relevance of the efforts by the Hypoxia Task

372   Force to reduce nitrogen pollution in the MARS. Further studies are needed to investigate river-

373   induced disturbances of the coastal carbonate system and to improve the still limited

374   understanding of the species tolerance to low Ω_{Ar} and pH levels in the region (Osborne et al.,

375   2022), so that suitable strategies for the management of marine resources can be developed.

376   Our findings add to an increasing number of regional modeling studies showing that river

377   runoff plays a key role as driver of carbonate variability in river influenced ocean margins (e.g.,

378   Siedlecki et al, 2017; Moore-Maley et al., 2018; Shen et al., 2020). In the northern GoM shelf,

379   river inputs are largely dominated by the MARS signature, but small rivers can also play a

380   significant role as drivers of Ω_{Ar} variability at a more local level (estuaries, bays). The system

381   could be especially sensitive to rivers along the states of Mississippi and Alabama (east of the

382   MARS delta), as those are characterized by much lower Alk:DIC ratios than the MARS (Gomez

383   et al., 2023), which would negatively impact Ω_{Ar}. It has been shown that El Nino-Southern

384   Oscillation (ENSO) influences the MARS discharge during winter, as well as discharges from

385   other northern GoM rivers during winter-spring, with El Nino periods associated with increased

386   river flow and La Niña periods with decreased river flow (e.g., Tootle et al., 2005; Gomez et al.,

387   2019). Consistently, our selected high (low) discharge winters for the composite analysis

388   coincide with El Nino (La Nina) periods during 2000-2019. This opens a potential for

389   predictability of the carbonate system disturbances in the northern GoM shelf, which deserves

390   further attention.

5 Conclusions

Based on model results, we showed that interannual changes in MARS discharge impact the carbonate system in the northern GoM inner-shelf, inducing significant Ω_{Ar} anomalies. Those changes are mainly driven by the mixing of river waters with a low Alk:DIC ratio, and increased biological production stimulated by the associated riverine nutrient input. The impact of the low buffer capacity on Ω_{Ar} is more pronounced during winter, while the impact of biologically driven processes is more important in summer. Sensitivity experiments suggested that the MARS's Alk:DIC ratio and nitrate concentration are key parameters influencing coastal carbonate variability in the northern GoM shelf. High discharge conditions increased the simulated fraction of coastal waters with Ω_{Ar} levels below two, thus increasing the vulnerability of calcifying organisms to OA.

Data Availability Statement

The model outputs used in this study can be found at the NOAA National Center for Environmental Information repository via https://www.ncei.noaa.gov/archive/accession/0277155. The ERA5 reanalysis product, the river chemistry data, and river discharge data were obtained at https://www.ecmwf.int/en/forecasts/dataset/ecmwf-reanalysis-v5, https://doi.org/10.25921/9jfw-ph50, and https://geo.gcoos.org/river_discharge, respectively.

References

Cai, W. J., Hu, X., Huang, W. J., Murrell, M. C., Lehrter, J. C., Lohrenz, S. E., et al. (2011), Acidification of subsurface coastal waters enhanced by eutrophication. *Nature Geoscience*, *4*(11), 766–770. https://doi.org/10.1038/ngeo1297

417   Doney, S. C., Fabry, V. J., Feely, R. A., & Kleypas, J. A. (2009), Ocean acidification: The other

418   CO2 problem. *Annual Review of Marine Science*, *1*, 169–192.

419   https://doi.org/10.1146/annurev.marine.010908.163834

420   Duarte, C. M., Hendriks, I. E., Moore, T. S., Olsen, Y. S., Steckbauer, A., Ramajo, L., et al.

421   (2013), Is ocean acidification an open-ocean syndrome? Understanding anthropogenic impacts

422   on seawater pH. *Estuaries and Coasts*, *36*(2), 221–236. https://doi.org/10.1007/s12237-013-

423   9594-3

424   Gomez, F. A., Lee, S. K., Hernandez Jr, F. J., Chiaverano, L. M., Muller-Karger, F. E., Liu, Y.,

425   & Lamkin, J. T. (2019), ENSO-induced co-variability of salinity, plankton biomass and coastal

426   currents in the northern Gulf of Mexico. Scientific reports, 9(1), 178.

427   https://doi.org/10.1038/s41598-018-36655-y

428   Gomez, F. A., Wanninkhof, R., Barbero, L., Lee, S. K., & Hernandez, F. J. (2020), Seasonal

429   patterns of surface inorganic carbon system variables in the Gulf of Mexico inferred from a

430   regional high-resolution ocean biogeochemical model. *Biogeosciences*, *17*, 1685–1700.

431   https://doi.org/10.5194/bg-17-1685-2020

432   Gomez, F. A., Lee, S.-K., Stock, C. A., Ross, A. C., Resplandy, L., Siedlecki, S. A., Tagklis, F.,

433   & Salisbury, J. E. (2023), RC4USCoast: a river chemistry dataset for regional ocean model

434   applications in the US East Coast, Gulf of Mexico, and US West Coast, Earth Syst. Sci. Data, 15,

435   2223–2234. https://doi.org/10.5194/essd-15-2223-2023.

436   Gruber, N., Clement, D., Carter, B. R., Feely, R. A., Van Heuven, S., Hoppema, M., et al.

437   (2019), The oceanic sink for anthropogenic CO2 from 1994 to 2007. *Science*, *363*(6432), 1193–

438   1199. https://doi.org/10.1126/science.aau5153

439   Guo, X., Cai, W.J., Huang, W.J., Wang, Y., Chen, F., Murrell, M.C., et al. (2012), Carbon

440   dynamics and community production in the Mississippi River plume. *Limnology and*

441   *Oceanography*, *57*(1), 1-17. https://doi.org/10.4319/lo.2012.57.1.0001

442   Hersbach, H., Bell, B., Berrisford, P., Hirahara, S., Horányi, A., Muñoz-Sabater, J., *et al.* (2020),

443   The ERA5 global reanalysis. Quarterly Journal of the Royal Meteorological Society, 146(730),

444   1999-2049. https://doi.org/10.1002/qj.3803

445 Hicks, T.L., Shamberger, K.E.F., Fitzsimmons, J.N. *et al.* (2022), Tropical cyclone-induced

446 coastal acidification in Galveston Bay, Texas. *Commun Earth Environ* 3, 297.

447 https://doi.org/10.1038/s43247-022-00608-1

448 Huang, W.J., Cai, W.J., Wang, Y., Lohrenz, S.E. & Murrell, M.C. (2015) The carbon dioxide

449 system on the Mississippi River-dominated continental shelf in the northern Gulf of Mexico: 1.

450 Distribution and air-sea CO2 flux. *Journal of Geophysical Research: Oceans*, *120*(3), 1429-

451 1445. https://doi.org/10.1002/2014JC010498

452 Huang W.J., Cai W.J., & Hu, X. (2021) Seasonal Mixing and Biological Controls of the

453 Carbonate System in a River-Dominated Continental Shelf Subject to Eutrophication and

454 Hypoxia in the Northern Gulf of Mexico. Front. Mar. Sci. 8:621243.

455 https://doi.org:10.3389/fmars.2021.621243

456 Joesoef, A., Kirchman, D. L., Sommerfield, C. K., & Cai, W.-J. (2017), Seasonal variability of

457 the inorganic carbon system in a large coastal plain estuary, Biogeosciences, 14, 4949–4963.

458 https://doi.org/10.5194/bg-14-4949-2017

459 Kealoha, A. K., Shamberger, K. E., DiMarco, S. F., Thyng, K. M., Hetland, R. D., Manzello, D.

460 P., et al. (2020), Surface water CO2 variability in the Gulf of Mexico (1996–2017), *Scientific

461 Reports*, *10*(1), 1–13. https://doi.org/10.1038/s41598-020-68924-0

462 Kekuewa, S. A. H., Courtney, T. A., Cyronak, T. *et al.* (2022), Seasonal nearshore ocean

463 acidification and deoxygenation in the Southern California Bight. *Sci Rep* **12**, 17969.

464 https://doi.org/10.1038/s41598-022-21831-y

465 Lacroix, F., Ilyina, T., Mathis, M., Laruelle, G. G., & Regnier, P. (2021), Historical increases in

466 land-derived nutrient inputs may alleviate effects of a changing physical climate on the oceanic

467 carbon cycle, Global change biology, 27(21), 5491-5513. https://doi.org/10.1111/gcb.15822

468 Lacroix, F., Ilyina, T., & Hartmann J. (2020), Oceanic CO_2 outgassing and biological production

469 hotspots induced by pre-industrial river loads of nutrients and carbon in a global modelling

470 approach, Biogeosciences, 17, 55–88. https://doi.org/10.5194/bg-17-55-2020

471 Laurent, A., Fennel, K., Cai, W.-J., Huang, W.-J., Barbero, L., & Wanninkhof, R. (2017),

472 Eutrophication- induced acidification of coastal waters in the northern Gulf of Mexico: Insights

473 into origin and processes from a coupled physical-biogeochemical model, Geophys. Res. Lett.,

474 44, 946–956. https://doi.org/10.1002/2016GL071881

475 Li, L., Stewart, B., Zhi, W., Sadayappan, K., Ramesh, S., Kerins, D., Sterle, G., Harpold, A., &

476 Perdrial, J. (2022), Climate controls on river chemistry. *Earth's Future*, *10*(6),

477 p.e2021EF002603. https://doi.org/10.1029/2021EF002603

478 Liu, Y., Lee, S. K., Enfield, D. B., Muhling, B. A., Lamkin, J. T., Muller-Karger, F. E., &

479 Roffer, M. A. (2015), Potential impact of climate change on the Intra-Americas Sea: Part-1: A

480 dynamic downscaling of the CMIP5 model projections. *Journal of Marine Systems*, *148*, 56–69.

481 https://doi.org/10.1016/j.jmarsys.2015.01.007

482 Liu, X., Stock, C.A., Dunne, J.P., Lee, M., Shevliakova, E., Malyshev, S., & Milly, P.C. (2021),

483 Simulated Global Coastal Ecosystem Responses to a Half-Century Increase in River Nitrogen

484 Loads. *Geophysical Research Letters*, *48*(17), p.e2021GL094367.

485 https://doi.org/10.1029/2021GL094367

486 Lohrenz, S. E., & Cai, W. J. (2006), Satellite ocean color assessment of air-sea fluxes of CO2 in

487 a river-dominated coastal margin. *Geophysical Research Letters*, *33*(1).

488 https://doi.org/10.1029/2005GL023942

489 Martínez-López, B., & Zavala-Hidalgo, J. (2009), Seasonal and interannual variability of cross-

490 shelf transports of chlorophyll in the Gulf of Mexico. *Journal of Marine Systems*, *77*, 1–20.

491 https://doi.org/10.1016/j.jmarsys.2008.10.002

492 Moore-Maley, B. L., Ianson, D., & Allen, S. E. (2018), The sensitivity of estuarine aragonite

493 saturation state and pH to the carbonate chemistry of a freshet-dominated river, Biogeosciences,

494 15, 3743–3760. https://doi.org/10.5194/bg-15-3743-2018

495 Muñoz-Salinas, E., & Castillo, M. (2015), Streamflow and sediment load assessment from 1950

496 to 2006 in the Usumacinta and Grijalva rivers (Southern Mexico) and the influence of ENSO.

497 *Catena*, *127*, 270–278. https://doi.org/10.1016/j.catena.2015.01.007

498 Orr, J., Fabry, V., Aumont, O. *et al.* (2005), Anthropogenic ocean acidification over the twenty-

499 first century and its impact on calcifying organisms. *Nature* 437, 681–686.

500 https://doi.org/10.1038/nature04095.

501   Osborne, E., Hu, X., Hall, E.R., Yates, K., Vreeland-Dawson, J., Shamberger, K., et al. (2022),

502   Ocean acidification in the Gulf of Mexico: Drivers, impacts, and unknowns. *Progress in*

503   *Oceanography*, p.102882. https://doi.org/10.1016/j.pocean.2022.102882

504   Rabalais, N. N., Turner, R. E., Sen Gupta, B. K., Boesch, D. F., Chapman, P., & Murrell, M. C.

505   (2007), Hypoxia in the northern Gulf of Mexico: Does the science support the plan to reduce,

506   mitigate, and control hypoxia? Estuar. Coast. 30, 753–772. https://doi.org/10.1007/BF02841332

507   Regnier, P., Resplandy, L., Najjar, R.G., & Ciais, P. (2022), The land-to-ocean loops of the

508   global carbon cycle, Nature, 603, 401–410. https://doi.org/10.1038/s41586-021-04339-9

509   Shchepetkin, A. F., & McWilliams, J. C. (2005), The regional oceanic modeling system

510   (ROMS): A split-explicit, free-surface, topography-following-coordinate oceanic model. *Ocean*

511   *Modelling*, *9*, 347–404. https://doi.org/10.1016/j.ocemod.2004.08.002

512   Shen, C., Testa, J. M., Li, M., & Cai, W.-J. (2020), Understanding anthropogenic impacts on pH

513   and aragonite saturation state in Chesapeake Bay: Insights from a 30-year model study. *Journal*

514   *of Geophysical Research: Biogeosciences*, *125*, e2019JG005620.

515   https://doi.org/10.1029/2019JG005620

516   Siedlecki, S. A., Pilcher, D. J., Hermann, A. J., Coyle, K., & Mathis, J. (2017), The importance

517   of freshwater to spatial variability of aragonite saturation state in the Gulf of Alaska. Journal of

518   Geophysical Research: Oceans, 122, 8482–8502. https://doi.org/10.1002/2017JC012791

519   Siedlecki, S. A., Salisbury, J., Gledhill, D. K., Bastidas, C., Meseck, S., McGarry, K., Hunt, C.

520   W., Alexander, M., Lavoie, D., Wang, Z. A., & Scott, J. (2021), Projecting ocean acidification

521   impacts for the Gulf of Maine to 2050: New tools and expectations, Elem Sci Anth, 9(1),

522   p.00062. https://doi.org/10.1525/elementa.2020.00062.

523   Tao, B., Tian, H., Ren, W., Yang, J., Yang, Q., He, R., Cai, W., & Lohrenz, S. (2014), Increasing

524   Mississippi river discharge throughout the 21st century influenced by changes in climate, land

525   use, and atmospheric CO2, Geophys. Res. Lett., 41, 4978–4986.

526   https://doi.org/10.1002/2014GL060361

527   Tootle, G. A., Piechota, T. C., & Singh, A. (2005), Coupled oceanic-atmospheric variability and

528   US streamflow. Water Resources Research, 41(12). https://doi.org/10.1029/2005WR004381

529   van Heuven, S. M. A. C., Pierrot, D., Rae, J. W. B., Lewis, E., & Wallace, D. W. R. (2011),

530   MATLAB program developed for CO2 system calculations. In *ORNL/CDIAC-105b. Carbon*

531   *Dioxide Information Analysis Center* (Vol. 530). Oak Ridge National Laboratory, US

532   Department of Energy. https://doi.org/10.3334/CDIAC/otg.CO2SYS_MATLAB_v1.1

533   von Storch, H. & Zwiers, F. W. (1999), *Statistical Analysis in Climate Research*, 484 pp,

534   Cambridge University Press. https://doi.org/10.1017/CBO9780511612336

535   Wang, Z. A., Wanninkhof, R., Cai, W. J., Byrne, R. H., Hu, X., Peng, T. H., & Huang, W. J.

536   (2013), The marine inorganic carbon system along the Gulf of Mexico and Atlantic coasts of the

537   United States: Insights from a transregional coastal carbon study. *Limnology & Oceanography*,

538   *58*, 325–342. https://doi.org/10.4319/lo.2013.58.1.0325

539   Wanninkhof, R., Barbero, L., Byrne, R., Cai, W. J., Huang, W. J., Zhang, J. Z., et al. (2015),

540   ocean Acidification along the Gulf Coast and east Coast of the USA. *Continental Shelf Research*,

541   *98*, 54–71. https://doi.org/10.1016/j.csr.2015.02.008

542   Yang, B., Byrne, R.H. & Wanninkhof, R. (2015), Subannual variability of total alkalinity

543   distributions in the northeastern Gulf of Mexico. *Journal of Geophysical Research: Oceans*,

544   *120*(5), pp.3805-3816. https://doi.org/10.1002/2015JC010780